



Paleoceanography and Paleoclimatology*



RESEARCH ARTICLE

10.1029/2021PA004405

Improved Model-Data Agreement With Strongly Eddyng Ocean Simulations in the Middle-Late Eocene

Peter D. Nootboom^{1,2} , Michiel Baatsen¹, Peter K. Bijl³, Michael A. Kliphuis¹, Erik van Sebille^{1,2} , Appy Sluijs³ , Henk A. Dijkstra^{1,2} , and Anna S. von der Heydt^{1,2} 

¹Department of Physics, Institute for Marine and Atmospheric Research Utrecht (IMAU), Utrecht University, Utrecht, The Netherlands, ²Centre for Complex Systems Studies, Utrecht University, Utrecht, The Netherlands, ³Department of Earth Sciences, Utrecht University, Utrecht, The Netherlands

Key Points:

- Eddyng ocean simulations provide a profoundly different local flow compared to noneddyng simulations
- Heat transport is enhanced in eddyng simulations leading to reduced equator-to-pole sea surface temperature gradients
- Eddyng simulations reduce model-data mismatches for sea surface temperature and ocean flow

Supporting Information:

Supporting Information may be found in the online version of this article.

Correspondence to:

P. D. Nootboom,
p.d.nootboom@uu.nl

Citation:

Nootboom, P. D., Baatsen, M., Bijl, P. K., Kliphuis, M. A., van Sebille, E., Sluijs, A., et al. (2022). Improved model-data agreement with strongly eddyng ocean simulations in the middle-late Eocene. *Paleoceanography and Paleoclimatology*, 37, e2021PA004405. <https://doi.org/10.1029/2021PA004405>

Received 13 DEC 2021
Accepted 21 JUL 2022

Author Contributions:

Conceptualization: Peter D. Nootboom, Michiel Baatsen, Peter K. Bijl, Michael A. Kliphuis, Erik van Sebille, Appy Sluijs, Henk A. Dijkstra, Anna S. von der Heydt
Data curation: Peter D. Nootboom, Michael A. Kliphuis
Formal analysis: Peter D. Nootboom
Funding acquisition: Peter K. Bijl, Erik van Sebille, Henk A. Dijkstra, Anna S. von der Heydt
Investigation: Peter D. Nootboom
Methodology: Peter D. Nootboom, Michiel Baatsen, Peter K. Bijl, Michael A. Kliphuis, Erik van Sebille, Appy

© 2022. The Authors.

This is an open access article under the terms of the [Creative Commons Attribution License](https://creativecommons.org/licenses/by/4.0/), which permits use, distribution and reproduction in any medium, provided the original work is properly cited.

Abstract Model simulations of past climates are increasingly found to compare well with proxy data at a global scale, but regional discrepancies remain. A persistent issue in modeling past greenhouse climates has been the temperature difference between equatorial and (sub-)polar regions, which is typically much larger in simulations than proxy data suggest. Particularly in the Eocene, multiple temperature proxies suggest extreme warmth in the southwest Pacific Ocean, where model simulations consistently suggest temperate conditions. Here, we present new global ocean model simulations at 0.1° horizontal resolution for the middle-late Eocene. The eddies in the high-resolution model affect poleward heat transport and local time-mean flow in critical regions compared to the noneddyng flow in the standard low-resolution simulations. As a result, the high-resolution simulations produce higher surface temperatures near Antarctica and lower surface temperatures near the equator compared to the low-resolution simulations, leading to better correspondence with proxy reconstructions. Crucially, the high-resolution simulations are also much more consistent with biogeographic patterns in endemic-Antarctic and low-latitude-derived plankton, and thus resolve the long-standing discrepancy of warm subpolar ocean temperatures and isolating polar gyre circulation. The results imply that strongly eddyng model simulations are required to reconcile discrepancies between regional proxy data and models, and demonstrate the importance of accurate regional paleobathymetry for proxy-model comparisons.

Plain Language Summary Climate models are widely used to understand warm climates in the geologic past such as the late Eocene (38 million years ago; ~8°C warmer than today). To determine the quality of these models, simulations are often compared to measured proxies representing the regional environment. Here, we show that a finer-than-typical detail in the ocean model causes a profoundly different regional ocean flow and environmental conditions. The improved correspondence to proxy data implies that high-resolution simulations are required for a meaningful point-by-point data-model comparison.

1. Introduction

Model-data comparisons for warm periods in the geological past can be used to test the performance of climate models under greenhouse conditions (Braconnot et al., 2012; Cramwinckel et al., 2018; Dowsett et al., 2013; Hutchinson et al., 2021; Kennedy-Asser et al., 2020; Liu et al., 2009; Lunt et al., 2021; Schmidt et al., 2014; Tabor et al., 2016; Tierney et al., 2020; Zhu et al., 2020). Some fully coupled climate models using state-of-the-art Eocene geographic boundary conditions (Baatsen et al., 2016) and greenhouse gas forcing simulate climates that correspond well to reconstructions of tropical sea surface temperature (SST) and deep ocean temperature (Cramwinckel et al., 2018). However, in such simulations, these models regionally simulate much cooler conditions in extratropical regions than proxy data suggest, particularly in the southwest Pacific (Baatsen et al., 2020; Cramwinckel et al., 2018; Huber & Caballero, 2011; Lunt et al., 2012, 2021). Consequently, depending on the radiative forcing, models either produce SSTs near the equator that are higher than proxy data indicate or SSTs at mid-to-high latitudes that are much lower than proxy reconstructions, leading to stronger meridional SST gradients.

One challenge in paleoclimate model-data comparisons is the scale difference between proxies and models. The proxies capture a regional environment and effects of small-scale regional setting (e.g., geography, bathymetry, and oceanography), while general circulation models have difficulties capturing regional climate correctly due to

Sluijs, Henk A. Dijkstra, Anna S. von der Heydt

Project Administration: Peter K. Bijl, Erik van Sebille, Henk A. Dijkstra, Anna S. von der Heydt

Resources: Erik van Sebille

Software: Peter D. Nootboom, Michael A. Kliphuis, Erik van Sebille, Anna S. von der Heydt

Supervision: Peter K. Bijl, Erik van Sebille, Henk A. Dijkstra, Anna S. von der Heydt

Validation: Peter D. Nootboom

Visualization: Peter D. Nootboom

Writing – original draft: Peter D. Nootboom

Writing – review & editing: Peter D. Nootboom, Michiel Baatsen, Peter K. Bijl, Michael A. Kliphuis, Erik van Sebille, Appy Sluijs, Henk A. Dijkstra, Anna S. von der Heydt

the coarse resolution that is typically used (1° horizontally or coarser for the ocean) (Dowsett et al., 2013; Eyring et al., 2019; Harrison et al., 2016; Kennedy-Asser et al., 2020; Nootboom et al., 2020; Tabor et al., 2016). The quality of ocean models improves considerably at a higher horizontal resolution (0.1°) (Dong et al., 2014; Griffies et al., 2015; Hewitt et al., 2016; McClean et al., 2006; Müller et al., 2019; Sun et al., 2019; Viebahn et al., 2016), especially their regional flow (Delworth et al., 2012; Marzocchi et al., 2015; Nootboom et al., 2020). This is not only due to higher level of detail, but also because of the smaller scale interactions resolved (including mesoscale eddies of 10–30-km size) that influence the large-scale flow properties (Porta Mana & Zanna, 2014) and increase the importance of the local setting (i.e., the paleogeography and bathymetry) in the resulting regional ocean flow.

Biogeographic patterns of microplankton (e.g., dinoflagellate cysts; dinocysts) in Southern Ocean marine sediments have been used as tracer of past surface oceanography (Huber et al., 2004). For instance, Eocene sediments deposited near Antarctica contain dinocyst species that are endemic to circum-Antarctic locations (Bijl et al., 2011). Hence, Southern Ocean regions with many of these endemic species, as opposed to those with abundant cosmopolitan species, must be oceanographically connected. This implies that these biogeographic patterns of dinocysts provide a direct proxy of the flow direction itself (Bijl et al., 2011). So far, climate models were broadly able to match the circulation patterns deduced from microplankton endemism in the Southern Ocean, sometimes after adaptations of the model paleobathymetry (Bijl et al., 2013; Houben et al., 2019; Huber et al., 2004) or details of the configuration of critical Southern Ocean gateways (Sijp et al., 2016). However, these model simulations cannot explain the occurrence or absence of endemic dinocysts at some sites. In addition, state-of-the-art fully coupled climate model simulations did come close to the proxy-based warmth in the southwest Pacific Ocean, but this required a flow through the Tasmanian Gateway which was incompatible with microplankton-based evidence of surface ocean flow (Cramwinckel et al., 2020; Stickley et al., 2004). Consequently, no model simulation exists that can reconcile southwest Pacific Ocean warmth with ocean flow that is compatible with the plankton records (Baatsen et al., 2020).

Model-data mismatches of ocean circulation and climate occur from the early to late Eocene (Bijl et al., 2013; Cramwinckel et al., 2018, 2020; Houben et al., 2019; Inglis et al., 2015; Stickley et al., 2004). Here, we show that high-resolution ocean model simulations partly solve this mismatch during the middle-late Eocene, using sinking Lagrangian particles to represent biogeographic patterns of microplankton in the ocean model simulations (Huber et al., 2004; Nootboom et al., 2019). We present the first simulations of a global eddying Eocene Ocean model with a 0.1° horizontal resolution (HR2 and HR4; Table 1). These simulations are initialized and forced with atmospheric fields from an equilibrium state of a coarser (1°) resolution model with a fully coupled ocean and atmosphere (LR2 and LR4; Table 1; Baatsen et al., 2020). Hence, the high-resolution and low-resolution simulations have a similar atmospheric forcing and bathymetry. The new high-resolution simulations are run for a few decades (42 and 27 years for HR2 and HR4, respectively), sufficient for the upper-ocean circulation to equilibrate. We focus on the middle-late Eocene in this paper, because of the availability of low-resolution simulations (Baatsen et al., 2020) and substantial field data of ocean circulation and climate during this time period.

2. Materials and Methods

2.1. Data

We used two data sets in this paper. The first includes the SST proxies from U_{37}^k , TEX_{86}^H , Mg/Ca, Δ_{47} and $\delta^{18}O$, which are described in detail in Baatsen et al. (2020). Proxy-based SST reconstructions come with uncertainties, limitations, and biases (Hollis et al., 2019), related to the depth, or season they represent. The second data set are sediment samples with dinocysts from Bijl et al. (2011), combined with the samples described in Bijl et al. (2021), Cramwinckel et al. (2020), and Houben et al. (2019). We averaged dinocyst abundance of Endemic-Antarctic, cosmopolitan and low-latitude-derived for the respective time slices.

2.2. Model Setup

We used the Parallel Ocean Program (POP; Smith et al., 2010) to perform eddying ocean model simulations for the middle-late Eocene (38 Ma). To derive the forcing of this model, we made use of the fully coupled (ocean and atmosphere) simulations with the Community Earth System Model v1.0.5 (CESM) from Baatsen et al. (2020), with a noneddying ocean. We used both CESM simulations with $2\times$ preindustrial atmospheric CO_2 (LR2) and $4\times$ preindustrial CO_2 (LR4) configuration. The setup of POP is similar to that in Viebahn et al. (2016), den Toom

Table 1
The Ocean Model Simulations of the Middle-Late Eocene (38 Ma) in This Paper

Run	Resolution	Layers	Type	Forcing ^a	Years run
LR2 ^a	1°	60	Fully coupled with atmosphere (CESM)	2× preindustrial CO ₂	3,000
LR4 ^a	1°	60	Fully coupled with atmosphere (CESM)	4× preindustrial CO ₂	4,000
HR2	0.1°	42	Ocean only (POP), forced by LR2 atmosphere	2× preindustrial CO ₂	42
HR4	0.1°	42	Ocean only (POP), forced by LR4 atmosphere	4× preindustrial CO ₂	27

^aFrom Baatsen et al. (2020).

et al. (2014), McClean et al. (2011), and Kirtman et al. (2012) with 42 vertical layers (Figure S1 in Supporting Information S1). The K-profile parameterization was used for vertical mixing.

The high-resolution POP is forced at the surface by a fixed atmosphere of the CESM simulation. To construct the surface forcing, we interpolated the average (over the last 50 model years of LR2 and LR4) SST, sea surface salinity (SSS), and wind stress (zonal and meridional) of the CESM simulation for every month of the year (such that a seasonal cycle is included in the surface forcing and determines most of the variability). These SST and SSS fields were used as restoring boundary conditions at the surface.

Restoring boundary conditions imply that POP is “pushed” toward the SST and SSS output of the CESM at the surface with a specific time scale (30 and 10²⁰ days, respectively). SSS is by approximation free to evolve due to the long restoring time scale, which implies that we use mixed boundary conditions in this paper. Typically, restoring boundary conditions allow for less SST variability compared to a configuration with a fully coupled atmosphere, since SST is pushed toward this fixed solution. The bathymetry that CESM uses was interpolated linearly on the high-resolution grid that POP uses, making both bathymetries similar (see the code at Nootboom (2022a)).

In order to investigate the sensitivity of simulations to model resolution, we choose a setup of the eddy model configurations which is as similar as possible to the noneddy model configurations. This means that the eddy simulations do not use a bathymetry which is more detailed compared to the noneddy simulations. The addition of a detailed bathymetry increases the bottom roughness, and hence has implications for the flow (Sauermilch et al., 2021).

For initialization of the eddy model, the three-dimensional ocean output at the end of the CESM simulations (LR2 and LR4) is interpolated to the higher resolution grid that POP (HR2 and HR4) uses. We simulated 42 and 27 years in total for HR2 and HR4, respectively. Since we investigate the response of the simulations to an increase in horizontal resolution, the same five model years of both HR2 and HR4 are used in most analyses in this paper: years 23–27. For the same analyses of the low-resolution simulations (LR2 and LR4), we used the last 5 years of these simulations.

Using this setup of POP, we can investigate the sensitivity of simulations to the studied resolution difference only, because the model is forced by the same atmosphere and their geographic boundary conditions are based on the same reconstruction of Baatsen et al. (2016), and the three-dimensional eddy ocean is initialized by the equilibrated output of the CESM. As a result, the atmosphere is representative of the middle-late Eocene climate, but does not respond to changes in the ocean. We hence cannot investigate the effect of atmospheric feedbacks on the results (Arzel et al., 2011; den Toom et al., 2012; Rahmstorf & Willebrand, 1995; Zhang et al., 2010).

Similar model setups of POP have been used in studies of the present-day, to study the response of overturning changes after surface freshwater perturbations (den Toom et al., 2014; Weijer et al., 2012), multidecadal variability (Le Bars et al., 2016) and sensitivity of the ocean heat transport to Southern Ocean gateway changes (Viebahn et al., 2016). Most of these studies show that ~100 years of spin-up is long enough for these present-day uncoupled eddy simulations to be in equilibrium in the upper to mid ocean, which is longer than the eddy simulations presented in this paper. In this paper, we study the response of the simulation to an increase in horizontal model resolution. Hence, we assume that the noneddy simulations, where the eddy simulations are based on, are in equilibrium and representative of the studied time period. Since we use Lagrangian particles, only the upper ocean should be in equilibrium, which is the case after ~15 years (Maltrud et al., 2010). The uncoupled

model setup may not represent ocean heat transport well at long time scales, since it implicitly assumes an atmosphere with infinite heat capacity, and the atmosphere of the noneddying simulations may not be compatible with the SST distribution in the eddying simulations (Huber et al., 2003).

The model setup is suited to study the effects of model resolution on Eocene Ocean flows, but it is not suitable to study dynamics which involve atmospheric coupling, such as the El Niño Southern Oscillation. The model setup can best be used to investigate the upper-ocean circulation, as the deep ocean is not in equilibrium yet. Therefore, we can only use this setup to obtain a transient response of the deep meridional overturning, not its equilibrium.

Since the restoring boundary conditions are fixed in the uncoupled POP simulations, the SST distribution is determined by a combination of these boundary conditions and internal heat transport within the ocean. Inconsistencies may arise between the direct ocean heat transport in the model and the implied ocean heat transport from the atmosphere, since the atmosphere is fixed (Huber et al., 2003), but cannot be avoided. We assume that this inconsistency is small in this paper compared to other studies that use OGCMs to test the sensitivity of ocean heat transport on gateway changes, where the deep ocean circulation typically changes more compared to the sensitivity to model resolution tested in this paper. The high model resolution itself does influence the thermocline depth (Small et al., 2014), however, and hence, the distribution of heat in the upper layers of the ocean.

The 38 Ma time slice paleogeography was chosen here, because it is also used by Baatsen et al. (2020), which our eddying simulations are based on. Moreover, suitable field data are provided for the middle-late Eocene Ocean circulation and climate, which allow us to properly test the effect of model resolution on the model-data agreement. HR2 is forced by an atmosphere with a CO₂ concentration that is representative for the 38 Ma time slice. HR4 is warmer, and since paleogeography did not change much throughout the Eocene (Lunt et al., 2021), HR4 is more representative of an earlier period in the Eocene (40–45 Ma) when geography was still similar (Baatsen et al., 2020).

2.3. Sinking Lagrangian Particles

To quantify sedimentary dinocyst endemism in the model, we applied a similar backtracking analysis of virtual sinking Lagrangian particles as in Nootboom et al. (2019) (Figure 1). We released these particles at the ocean bottom and tracked them back in time while sinking and being advected by the three-dimensional flow from POP, until they reached 10-m depth. We released particles on a 2° × 1° grid of locations between 32°S and 80°S every day for a year and waited until all of the particles reached the near-surface (i.e., 17,520 particles in total). This analysis requires a higher than monthly temporal resolution of model output (Nootboom et al., 2020; Qin et al., 2014). Therefore, we used daily fields for the years 35–42 (HR2) and years 20–27 (HR4) to perform this backtracking analysis.

We used a particle sinking speed of 6 m day⁻¹ for the Lagrangian particles in this paper. This represents a low sinking speed for single dinocysts (Anderson et al., 1985). We choose this low sinking speed, because it is considered as a lower bound of the realistic sinking speeds where most lateral transport occurs, which makes it easier to explain low abundances of dinocyst species. However, this sinking speed could in reality be different due to, e.g., aggregation with other particles. We also applied a sinking speed of 25 m day⁻¹ (see Figure S2 in Supporting Information S1), which represent small aggregates (Nootboom et al., 2019). The main conclusions on the model-data comparison do not change if 25 m day⁻¹ instead of 6 m day⁻¹ sinking speed is used.

This paper follows previous assumptions (Huber et al., 2004) that the biogeographic distribution of Antarctic endemism was temperature-controlled. Bijl et al. (2011) recognized that the biogeographic distribution of Antarctic-endemic dinocysts followed the broad pattern of gyral ocean circulation in the Eocene, in both the South Pacific and the South Atlantic. This implied dominance of endemism in the northward flowing western boundary currents in the southwest Pacific and Atlantic. This paper assumes that presence of Antarctic-endemic dinocysts outside “cold” regions must have been the result of lateral transport through ocean currents (following the approach of Nootboom et al. (2019)). Although this is not in disagreement with Bijl et al. (2011), it assigns a larger role to lateral transport instead and a tighter temperature tolerance to endemic dinocysts than in Bijl et al. (2011).

The percentage of dinocyst endemism in the model is determined by the percentage of particles that originated from an environment with a temperature below \overline{SST} when it reaches the surface (which must be close to Antarc-

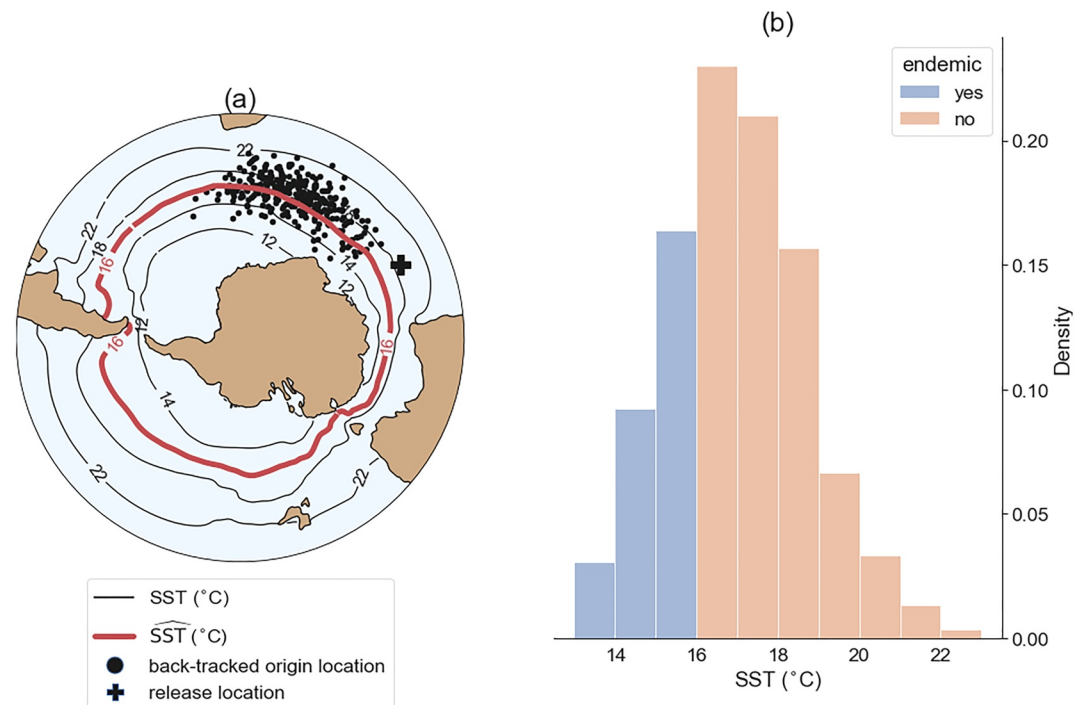


Figure 1. Illustration of the modeled dinocyst endemism near Antarctica. (a) Virtual particles are released at the bottom release location and tracked back in time with some sinking speed to determine their surface origin location. If the sea surface temperature (SST) at the back-tracked origin location is lower than the threshold SST ($\widehat{SST} = 16^{\circ}\text{C}$ in this illustration), it is assumed to originate close to Antarctica; hence, it is flagged as endemic. (b) A histogram of SSTs at the surface origin locations.

tica; similar approach as in Huber et al. (2004)). The percentage of modeled dinocyst endemism is not expected to compare well with the percentage of measured endemic dinocyst, because this match is also sensitive to the species-specific susceptibility of dissolution during the sinking journey and their productivity at the ocean surface (Nooteboom et al., 2019). Therefore, we compare whether any endemic species occur in sites (0% or >0%) between model and data instead of the exact percentage.

We assume that the sinking Lagrangian particles are not greatly influenced by the fact that the deep circulation is not in full equilibrium yet in the eddy simulations. Most of the lateral particle displacement occurs near the surface which is in equilibrium and where the currents are the strongest. Moreover, the eddy simulations are initialized with output from the noneddy simulations, which are in reasonable equilibrium. The mechanistic development of the flow, given the heat and salt distribution from the initialization, occurs in a few years (see also Figures 4c–4h). Hereafter, the flow changes slowly and may equilibrate after $\sim 1,000$ years due to the flow response to changing density distributions. The assumption that sinking Lagrangian particles are not greatly affected by the deep ocean equilibration is supported by the results that use sinking Lagrangian particles in HR2 and HR4: These results are similar, even though the deep ocean circulation is different in HR2 and HR4.

3. Effect of Model Resolution on Eocene Flow

The resulting ocean circulation is different between the eddy and noneddy configurations (Figure 2). In the eddy simulations, the time-mean flow strength has a higher spatial variability, the bathymetry has a larger influence on the flow strength and direction (especially in the Southern Ocean; see Figure S3 in Supporting Information S1 for the bathymetry), and local scale features are much more pronounced, compared to the low-resolution model. All western boundary and equatorial currents increase in strength, except in the North Atlantic. The spatial structure and separation locations of the western boundary currents are also shifted. For instance, the eastward Agulhas separation (near South-Africa) is only present in the eddy simulations (it retroflects more eastward compared to the present-day). Moreover, east of Australia, the East Australia Current

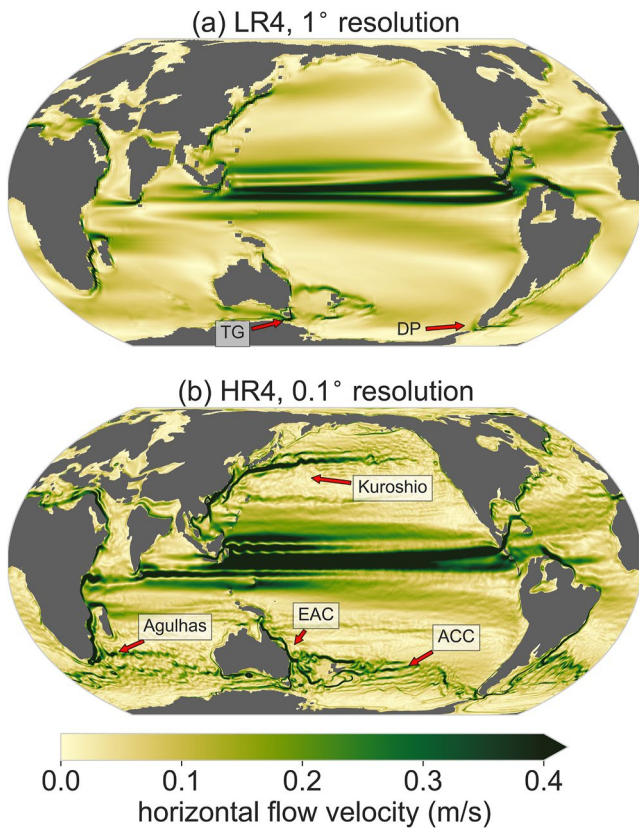


Figure 2. Magnitude of the time-mean surface horizontal flow velocity in the model of (a) 1° (mean over years 3995–4000) and (b) 0.1° horizontal resolution (mean over years 23–27). Both with 4× preindustrial atmospheric CO₂ (LR4 and HR4). See Figure S4 in Supporting Information S1 for the barotropic stream functions in all configurations. The Drake Passage (DP), Tasman Gateway (TG), East Australian Current (EAC), Kuroshio current, and proto-Antarctic Circumpolar Current (ACC) are labeled.

(EAC) extends further southeastwards in the eddying compared to the noneddy simulation, while there is a narrow but strong northward current east of Tasmania that is not present in the low-resolution simulations.

The EAC flow provides an example of the stronger influence of the paleobathymetry on the flow in HR4 compared to LR4, even though the bathymetry is the same in both configurations. Eddies are responsible for the downward transfer of momentum input at the ocean surface by winds that is eventually balanced by bottom form stresses (Munday et al., 2015). As a consequence, the flow is strongly determined by isobaths (i.e., lines of constant bathymetry; Marshall, 1994; Rintoul, 2018). Hence, the bathymetry has a much larger influence on the flow if the ocean is eddying (in HR4 and HR2) than if it is not (LR2 and LR4). In HR4, the EAC is steered further southeastward than in LR4 along the submerged continental block of Lord Howe Rise (see Figure S3 in Supporting Information S1 for the bathymetry). Moreover, jets like the EAC have a narrower structure in the eddying flow, due to interactions between eddies and the time-mean flow (Waterman et al., 2011), which has profound impacts on the regional oceanography.

3.1. Model-Data Comparison: Plankton Biogeography

The new Eocene Ocean model velocity fields enable the use of sinking Lagrangian particles (Nooteboom et al., 2020) to reveal biogeographic provinces of endemic microplankton in the Eocene Southern Ocean. In this way, we can test how representative the modeled flow is compared with the reconstructed ocean flow from sediment records. In this approach, it is determined where sedimentary particles originated from at the ocean surface, while taking into account how the particles were advected by ocean currents during their sinking journey. If these virtual particles originate from an environment with a temperature below a threshold value indicated by \widehat{SST} (see Section 2 and Figure 1), the particle is assumed to originate close to Antarctica, and flagged as representing Antarctic-endemic dinocyst species (see Section 2 and Figure 1 for an illustration). As such, model dinocyst endemism at the ocean bottom is determined by the percentage of virtual particles that started sinking in a surface environment with a temperature below \widehat{SST} (Figure 3).

Due to the circulation differences between eddying and noneddy simulation, the model-derived occurrence of Antarctic-endemic sedimentary dinocysts is clearly different between both configurations (Figure 3). While the endemism is more strongly dependent on latitude and a sharper boundary exists between low-endemism and high-endemism in LR4, sinking particles are transported further away from Antarctica in specific areas (especially near western boundary currents) in HR4. As a consequence, the occurrence of several recorded endemic species can be explained in HR4, while it cannot in LR4 (see e.g., site SanB). Moreover, the modeled endemism in the noneddy LR4 cannot match with both DSDP277 and MH at the same time, because these sites contain an opposite signal (i.e., MH contains endemic species and DSDP277 does not) while being located closely to each other. In HR4 on the other hand, the sedimentary particles in site DSDP277 (Figure 3) originate only from the warm waters of the southeastward flowing EAC, while the closely located site MH also contains particles originating from cold waters in the east, in agreement with the occurrence of endemic species at MH.

Overall, we find that the eddying model is able to produce a flow pattern which is consistent with plankton biogeographic patterns at all sites (Figures 3a and 3b). The model-data fit improvement in HR4 compared to LR4 highlights the need for accurate reconstructions of the geographic boundary conditions (Baatsen et al., 2016) to optimize model-data matches as in Figures 3a and 3b: It is the details in the ocean flow that induce a better model-data fit in HR4 compared to LR4.

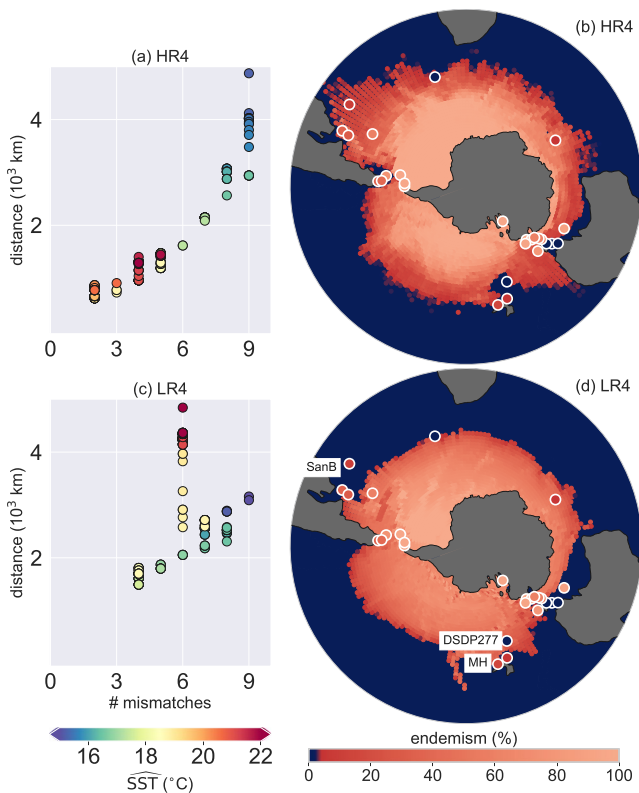


Figure 3. Model-data comparison: Antarctic endemism of sedimentary dinocysts in configurations HR4 and LR4. Both HR4 and LR4 are compared to 27 sites in total. The model dinocyst endemism at the ocean bottom is determined by the percentage of virtual particles that started sinking (with 6 m day^{-1} sinking speed) in a surface environment with temperature below \overline{SST} (see Figure 1 for an illustration). (a, c) Model-data fit for HR4 and LR4, respectively, for different values of \overline{SST} (given by the dot colors). Model and data compare better if the following two measures of fit are lower: (1) the number of sites with a point-to-point model-data mismatch in terms of endemic dinocyst species occurrence and (2) shortest cumulative distance of these sites to a location in the model that does match in terms of endemic dinocyst occurrence (i.e., $\sum_i D_i$, where D_i is the distance between a site i and a location in the model that does match with site i in terms of the endemic dinocyst occurrence). (b, d) Model-data comparison of dinocyst endemism at the \overline{SST} value that minimizes the measures of fit in (a) and (c). The sedimentary endemism of the data is the percentage of measured endemic species at the site (Bijl et al., 2011), representative of 41–39 Ma. Labeled sites are named in the main text.

The modeled dinocyst endemisms in the 2× and 4× preindustrial atmospheric CO_2 configurations are similar (see Figures S2, S5, and S6 in Supporting Information S1), even though HR2 and HR4 are forced by a different atmosphere and respond differently after initialization (Figure 4). However, the transient response of the upper-ocean equilibrates similarly in the 2× and 4× preindustrial CO_2 cases in a few decades, which also results in a similar time-mean surface flow (Figure S7 in Supporting Information S1). This implies that plankton biogeographic patterns and surface ocean circulation are to a large extent affected by bathymetry, rather than the climate boundary conditions (e.g., atmospheric CO_2) of the model.

At the beginning of the HR2 and HR4 simulations, much of the energy input at the surface is used to set up the circulation and the development of eddies, as can be seen from a reduction of Southern Ocean gateway transports in the first 5 years (similar in both HR2 and HR4), after which they recover (Figures 3c–3f). The reduced Southern Ocean gateway transport is caused by the growing eddy field, which extracts potential energy from the stratification and reduces the isopycnal slopes (Figure S8 in Supporting Information S1). However, the gateway transports recover after 5 years. The Drake Passage transport (through the gateway between South America and Antarctica) exceeds the transport in the low-resolution simulations after 9 years and equilibrates at a higher level. The increased Drake Passage transport could be caused by the lower (more realistic) viscosity that the high-resolution models allow compared to the low-resolution model (which becomes numerically unstable at this low viscosity value), while isopycnals do not necessarily become steeper compared to the noneddy simulations. Interestingly, the volume transport through the Tasman Gateway in HR2 and HR4 does not exceed the volume transport in LR2 and LR4. Instead, a larger fraction of the water is transported north of Australia, resulting in the stronger southeastward East Australian Current (EAC) in the South Pacific (Figure 2).

3.2. Model-Data Comparison: SST

Now that the high-resolution POP model simulates an Eocene Ocean flow, which is consistent with proxy data for ocean circulation, we compare the results of these simulations to proxy data for SST. SST distributions, however, are also influenced by the model background state and sensitive to their global-scale equilibration. Moreover, the background flow affects the distribution of heat differently in the eddying versus noneddy simulations. Mesoscale eddies are important for the distribution of heat, and eddying ocean models do a better job in representing heat transport compared to noneddy models that use parameterizations for eddy-induced heat transport (Dong et al., 2014; Griffies et al., 2015; Viebahn et al., 2016).

Indeed, heat change is distributed differently in the upper km of the eddying compared to the noneddy simulations (Figures 4a and 4b). Eddies efficiently transport heat to the subsurface (Delworth et al., 2012), which leads to subsurface warming in both eddying simulations (HR2 and HR4) and a lower vertical temperature gradient compared to LR2 and LR4. However, in HR2, the surface cools more, while the subsurface warms less compared to HR4.

Much of the heat transport change from LR to HR is related to the Southern and Northern Meridional Overturning Circulation (SMOC and NMOC, respectively), which has implications for the SST model-data comparison. In both HR2 and HR4, North Pacific sinking develops (in a few decades) next to existing South Pacific sinking, while in the low-resolution simulations there is only Southern Hemisphere sinking (see Figure S9 in Supporting Information S1). Overall, the North Pacific sinking leads to an increase in the NMOC and a decrease in the

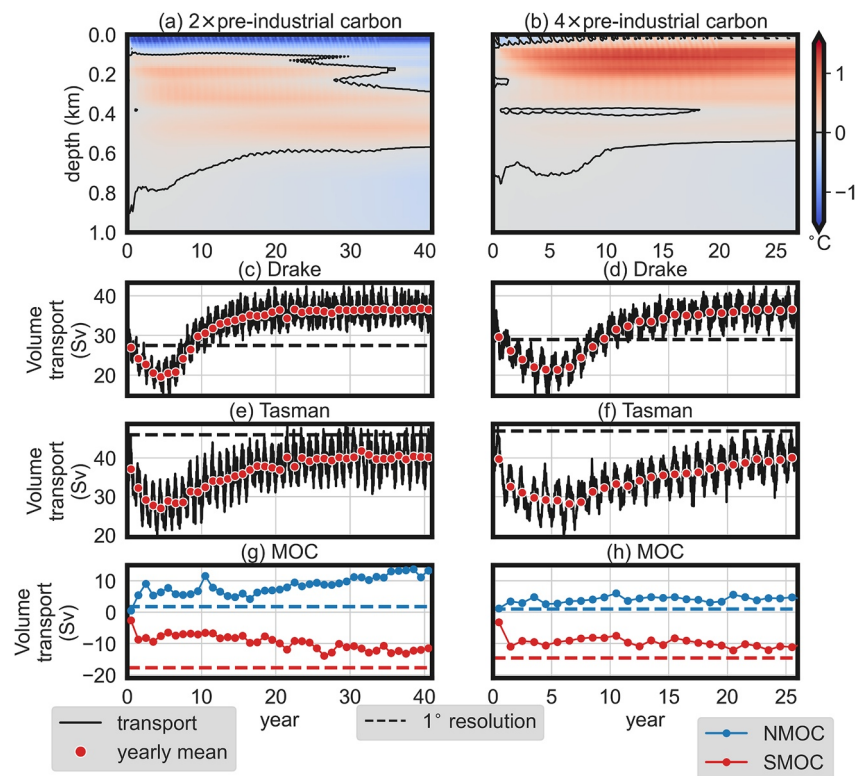


Figure 4. Response of the ocean model after initialization, HR2 (left) and HR4 (right). Note that the initial state of HR2 (HR4) corresponds to LR2 (LR4). (a, b) Depth-dependent evolution of the horizontal mean temperature increase compared to the initialization state (upper 1 km only). Water volume transport through the (c, d) Drake Passage (65°W) and (e, f) Tasman Gateway (150°E). (g, h) Maximum of the northern and southern zonal mean meridional overturning. MOC, Meridional Overturning Circulation; NMOC, Northern MOC; SMOC, Southern MOC; Sv, Sverdrup.

SMOC. These changes in the MOC are stronger in HR2 compared to HR4, and both the NMOC and SMOC are still increasing in magnitude at the end of the HR2 simulation.

The SMOC also differs in structure between the high-resolution and low-resolution simulations (see the mixed layer depth in Figure S9 in Supporting Information S1). In HR2 and HR4, more volume transport through Drake Passage increases the surface salinity in the South Atlantic resulting in denser surface water in the Weddell Sea (Tumoulin et al., 2020). Therefore, the main deepwater formation location is the South Atlantic in HR2 and HR4, while it is the South Pacific in LR2 and LR4.

These results imply that HR2 and HR4 are run long enough for the upper-ocean circulation to equilibrate, while the deep ocean is not in equilibrium yet, as can be seen from the MOC in HR2 (Figure 4g). Although the transient evolution of the deep ocean circulation differs between HR2 and HR4, we can nevertheless investigate their impact on SST distributions and compare these to proxy data.

Both the tropical and Arctic Ocean cool significantly in HR2 compared to LR2, while in HR4, the equatorial regions cool less and high-latitude (north and south) regions warm more as compared to LR4 (see Figure 5). For both atmospheric CO₂ levels, local SST differences between the high-resolution and low-resolution simulations mostly occur near western boundary currents of which the location shifts in the eddying simulation (Figures 5a and 5d). These shifts have an effect on the model-data comparison at sites near western boundary currents. In fact, the EAC transports warm waters southeastwards in the southwest Pacific, which (partly) explains why sites in the southwest Pacific are found to be warmer compared to model simulations with a coarse resolution, which has been speculated to be a reason for the model-data mismatch in the southwest Pacific before (Hollis et al., 2012). Notably, similar SST changes occur near the Kuroshio and Agulhas currents. The Weddell Sea warms up in HR2 and HR4 compared to LR2 and LR4, respectively, which is related to the South Atlantic sinking that occurs in HR2 and HR4.

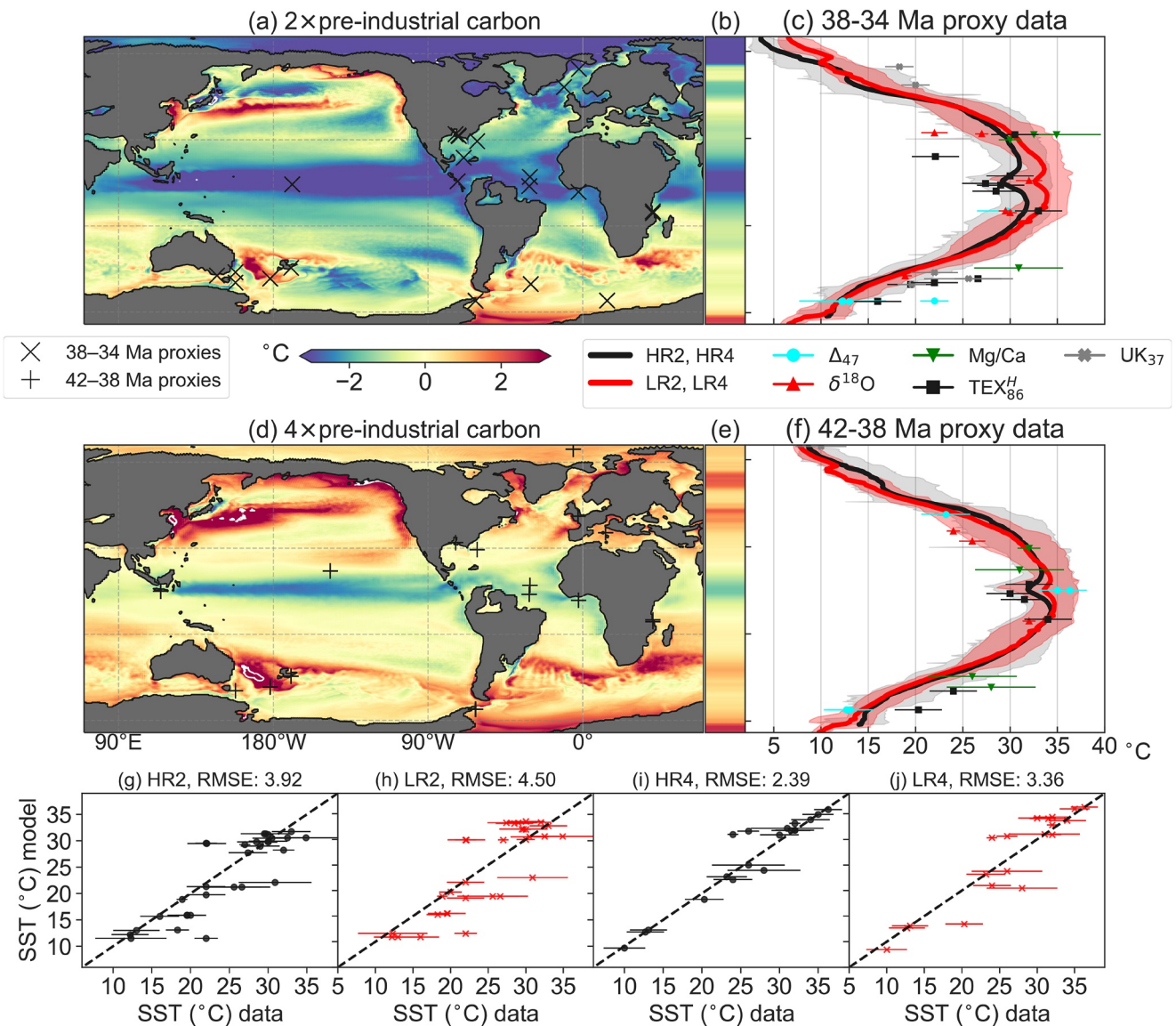


Figure 5. Model-proxy data comparison: sea surface temperature (SST). The 2× and 4× preindustrial case are compared to SST proxy data of 38–34 and 42–38 Ma, respectively. (a, d) SST difference of the high-resolution compared to the low-resolution model with the site locations of the SST proxies for 2× and 4× preindustrial carbon configuration, respectively, and (b, e) their zonal mean. Solid white lines indicate $\pm 5^\circ\text{C}$ contours. (c, f) the zonally averaged annual mean SST in the high-resolution (black) and the low-resolution (red) model for 2× and 4× preindustrial carbon configuration, respectively. The shaded areas show zonal spread (i.e., minimum and maximum) of the annual mean SST. Markers indicate SST proxy estimates with their uncertainty. (g–j) Scatter plots between proxy-derived and model-derived SST for all four configurations, with root mean squared errors (RMSE). Error bars represent proxy calibration errors. To consider the paleolocation uncertainty of sites (van Hinsbergen et al., 2015), each site is compared to the model SST value from up to 3° distance of the site that minimizes the RMSE of the scatter plot (similar to Baatsen et al. (2020); see Figure S10 in Supporting Information S1 for a point-to-point comparison). The dashed black line is the one-to-one line representing the perfect match between model and proxy data.

Climate models generally do not produce the low meridional temperature gradients of warm climates as inferred from proxy data (Huber & Caballero, 2011; Sijp et al., 2014). While the simulations LR2 and LR4 were found to generate a lower meridional SST gradient compared to other models of 1° horizontal resolution or coarser (Baatsen et al., 2020), this gradient reduces further in HR2 and HR4. The tropics are cooler in HR2 and HR4 compared to LR2 and LR4, while in the zonal mean the southern high latitudes are only slightly warmer in HR4 (Figures 5d–5f). Regionally, there is, however, significant warming of Southern Ocean SSTs in HR4. Overall, this improves consistency between the high-resolution model results and SST proxies in the tropics, while the modeled high-latitude SST values are often still lower than the proxy-derived SST values. The eddy simulations show

stronger horizontal gradients in the time-mean SST field compared to the noneddy simulations, which results in a higher time-mean SST variation in the model around the sediment sample sites. The model-data fit greatly improves in the eddy simulation compared to noneddy simulations (Figures 5g–5j), although a mismatch with some sites remains (especially for the 2× preindustrial CO₂ case) and the high-latitude temperatures are overall lower compared to the proxy data.

Overall, the eddy ocean model improves the SST model-data match from the noneddy model, because it alters the local transport of heat. However, the SST model-data comparison is also sensitive to the model background state (i.e., the state of the ocean at a global scale), which depends on the used atmospheric forcing, paleogeography and long time scales phenomena, such as the deep meridional overturning circulation. Hence, the SST model-data mismatch could be reduced even further if better model boundary conditions are used which lead to a more realistic background state of the late Eocene.

4. Conclusion and Outlook

We have shown that an eddy Eocene Ocean simulation provides a more detailed ocean flow compared to a noneddy version of the same model. As a result, model-data mismatches in the geologic past (Baatsen et al., 2020; Bijl et al., 2011; Houben et al., 2019; Huber et al., 2004; Hutchinson et al., 2021; Lunt et al., 2021) can at least partly be explained by the lack of eddies in the ocean models used. Our eddy simulations of the late Eocene are better able to explain the occurrence or absence of endemic dinocyst species near Antarctica compared to noneddy simulations. The SST model-data comparison also improved in the eddy simulation compared to noneddy simulations.

The explicit representation of eddies in ocean models may have implications for comparison of models with other proxy types than considered here. For instance, pollen-based temperature reconstructions imply that it did not freeze at the Antarctic coast during winter in the early Eocene (globally ~6 °C warmer than the late Eocene), despite polar darkness (Pross et al., 2012). Eddy-induced flow, and its impact on ocean heat transport, could in part explain such conditions.

The simulations in this paper are computationally expensive. However, other types of model setups may be interesting if computational capabilities are available. The strong influence of bathymetry on the eddy flow implies that the uncertainty of paleogeography reconstructions will have a major impact on model-data comparisons. Future studies could make adaptations to the bathymetry within uncertainty of paleogeographic reconstructions, to find its impact on the modeled ocean circulation and model-data comparison. These adaptations could also include more detail in the bathymetry, similar to Sauermlch et al. (2021).

Moreover, since the eddy flow has a direct response to bottom topography, it seems suitable for a downscaling, or eddy parameterization type of approach to obtain this influence of bathymetry on the flow with reduced computational costs. However, these type of approaches are found to be challenging in present-day configurations (Fox-Kemper et al., 2019; Lanzante et al., 2018; Nooteboom et al., 2020).

Second, we used the model equilibrium of the noneddy climate model simulations (which are in radiative equilibrium (Baatsen et al., 2020)) to start and force the eddy model. However, this switch induces a drift of the deep ocean circulation, which is not equilibrated yet in the high-resolution simulations of this paper. Hence, the background state of the model will change further if the model is run for longer time periods (a few millennia). Future simulations may have the capabilities to perform longer simulations. These changes of the model background state on long time scales might have implications for the regional flow and the quality of the model-data comparisons.

Finally, atmospheric feedbacks greatly influence the ocean model background state on long time scales, such as the meridional overturning circulation (Arzel et al., 2011; den Toom et al., 2012; Rahmstorf & Willebrand, 1995; Zhang et al., 2010). Hence, the high-resolution ocean should be coupled to a high-resolution atmosphere, which could further enhance the meridional transport of heat and lead to an improved model-data comparison. So far, it has been shown that ocean-atmosphere coupling in low-resolution models does not necessarily lead to more poleward heat transport in an Eocene climate compared to the present-day (Huber & Nof, 2006). However, coupling of the ocean with a high-resolution atmosphere may result in relevant changes of the poleward heat transport, for instance due to resolving small-scale features in the atmosphere such as tropical cyclones (Scoccimarro

et al., 2011). An eddy-permitting ocean could help facilitate a better overall match to SST observations in a fully coupled configuration, as it did in the present-day (Delworth et al., 2012).

Data Availability Statement

The code used for this work and the results are distributed under the MIT license (Nootboom, 2022a). The model data used to generate the main figures in this paper are publicly available on the Utrecht University Yoda platform (Nootboom, 2022b).

Acknowledgments

This work was funded by the Netherlands Organization for Scientific Research (NWO), Earth and Life Sciences, through project ALWOP.207 and supported by the Netherlands Earth System Science Center. The use of SURFsara computing facilities was sponsored by NWO-EW (Netherlands Organization for Scientific Research, Exact Sciences) under the project 17189 and 2020.022. PKB and AS thank the European Research Council for ERC starting Grant #802835 (OceaNice) and Consolidator Grant #771497 (SPANC), respectively.

References

- Anderson, D. M., Lively, J. J., Reardon, E. M., & Price, C. A. (1985). Sinking characteristics of dinoflagellate cysts. *Limnology and Oceanography*, 30(5), 1000–1009. <https://doi.org/10.4319/lo.1985.30.5.1000>
- Arzel, O., England, M. H., & Saenko, O. A. (2011). The impact of wind stress feedback on the stability of the Atlantic meridional overturning circulation. *Journal of Climate*, 24, 1965–1984. <https://doi.org/10.1175/2010JCLI13137.1>
- Baatsen, M., Heydt, A. S. V. D., Huber, M., Kliphuis, M. A., Bijl, P. K., Sluijs, A., & Dijkstra, H. A. (2020). The middle to late Eocene greenhouse climate modelled using the CESM 1.0.5. *Climate of the Past*, 16, 2573–2597. <https://doi.org/10.5194/cp-16-2573-2020>
- Baatsen, M., Van Hinsbergen, D. J. J., Von Der Heydt, A. S., Dijkstra, H. A., Sluijs, A., Abels, H. A., & Bijl, P. K. (2016). Reconstructing geographical boundary conditions for palaeoclimate modelling during the Cenozoic. *Climate of the Past*, 12(8), 1635–1644. <https://doi.org/10.5194/cp-12-1635-2016>
- Bijl, P. K., Bendle, J. A. P., Bohaty, S. M., Pross, J., Schouten, S., Tauxe, L., et al. (2013). Eocene cooling linked to early flow across the Tasmanian Gateway. *Proceedings of the National Academy of Sciences of the United States of America*, 110(24), 9645–9650. <https://doi.org/10.1073/pnas.1220872110>
- Bijl, P. K., Frieling, J., Cramwinckel, M., Boschman, C., Sluijs, A., & Peterse, F. (2021). Maastrichtian-Rupelian paleoclimates in the southwest Pacific—A critical evaluation of biomarker paleothermometry and dinoflagellate cyst paleoecology at Ocean Drilling Program Site 1172. *Climate of the Past*, 17(6), 6. <https://doi.org/10.5194/cp-17-2393-2021>
- Bijl, P. K., Pross, J., Warnaar, J., Stickley, C. E., Huber, M., Guerin, R., et al. (2011). Environmental forcings of paleogene Southern Ocean dinoflagellate biogeography. *Paleoceanography*, 26, PA1202. <https://doi.org/10.1029/2009PA001905>
- Braconnot, P., Harrison, S. P., Kageyama, M., Bartlein, P. J., Masson-delmotte, V., Abe-ouchi, A., et al. (2012). Evaluation of climate models using palaeoclimatic data. *Nature Climate Change*, 2, 417–424. <https://doi.org/10.1038/nclimate1456>
- Cramwinckel, M. J., Huber, M., Kocken, I. J., Agnini, C., Bijl, P. K., Bohaty, S. M., et al. (2018). Synchronous tropical and polar temperature evolution in the Eocene. *Nature*, 559, 382–386. <https://doi.org/10.1038/s41586-018-0272-2>
- Cramwinckel, M. J., Woelders, L., Huurdeman, E. P., Peterse, F., Gallagher, S. J., Pross, J., et al. (2020). Surface-circulation change in the southwest Pacific ocean across the middle Eocene climatic optimum: Inferences from dinoflagellate cysts and biomarker paleothermometry. *Climate of the Past*, 16, 1667–1689.
- Delworth, T. L., Rosati, A., Anderson, W., Adcroft, A. J., Balaji, V., Benson, R., et al. (2012). Simulated climate and climate change in the GFDL CM2.5 high-resolution coupled climate model. *Journal of Climate*, 25, 2755–2781. <https://doi.org/10.1175/jcli-d-11-00316.1>
- den Toom, M., Dijkstra, H. A., Cimadoribus, A. A., & Drijfhout, S. S. (2012). Effect of atmospheric feedbacks on the stability of the Atlantic meridional overturning circulation. *Journal of Climate*, 25, 4081–4096. <https://doi.org/10.1175/jcli-d-11-00467.1>
- den Toom, M., Dijkstra, H. A., Weijer, W., Hecht, M. W., Maltrud, M. E., & van Sebille, E. (2014). Response of a strongly eddying global ocean to north Atlantic freshwater perturbations. *Journal of Physical Oceanography*, 44(2), 464–481. <https://doi.org/10.1175/jpo-d-12-0155.1>
- Dong, C., McWilliams, J. C., Liu, Y., & Chen, D. (2014). Global heat and salt transports by eddy movement. *Nature Communications*, 5, 3294. <https://doi.org/10.1038/ncomms4294>
- Dowsett, H. J., Foley, K. M., Stoll, D. K., Chandler, M. A., Sohl, L. E., Bentsen, M., et al. (2013). Sea surface temperature of the mid-Piacenzian ocean: A data-model comparison. *Scientific Reports*, 3, 2013. <https://doi.org/10.1038/srep02013>
- Eyring, V., Cox, P. M., Flato, G. M., Gleckler, P. J., Abramowitz, G., Caldwell, P., et al. (2019). Taking climate model evaluation to the next level. *Nature Climate Change*, 9, 102–110. <https://doi.org/10.1038/s41558-018-0355-y>
- Fox-Kemper, B., Adcroft, A., Böning, C. W., Chassignet, E. P., Gerdes, R., Greatbatch, R. J., et al. (2019). Challenges and prospects in ocean circulation models. *Frontiers in Marine Science*, 6, 65. <https://doi.org/10.3389/fmars.2019.00065>
- Griffies, S. R., Winton, M., Anderson, W. G., Benson, R., Delworth, T. L., Dufour, C. O., et al. (2015). Impacts on ocean heat from transient mesoscale eddies in a hierarchy of climate models. *Journal of Climate*, 28, 952–977. <https://doi.org/10.1175/jcli-d-14-00353.1>
- Harrison, S. P., Bartlein, P. J., & Prentice, I. C. (2016). What have we learnt from palaeoclimate simulations? *Journal of Quaternary Science*, 31, 363–385. <https://doi.org/10.1002/jqs.2842>
- Hewitt, H. T., Roberts, M. J., Hyder, P., Graham, T., Rae, J., Belcher, S. E., et al. (2016). The impact of resolving the Rossby radius at mid-latitudes in the ocean: Results from a high-resolution version of the met office GC2 coupled model. *Geoscientific Model Development*, 9, 3655–3670. <https://doi.org/10.5194/gmd-9-3655-2016>
- Hollis, C., Taylor, K., Handley, L., Pancost, R., Huber, M., Creech, J., et al. (2012). Early paleogene temperature history of the southwest Pacific ocean: Reconciling proxies and models. *Earth and Planetary Science Letters*, 349–350, 53–66. <https://doi.org/10.1016/j.epsl.2012.06.024>
- Hollis, C. J., Dunkley Jones, T., Anagnostou, E., Bijl, P. K., Cramwinckel, M. J., Cui, Y., et al. (2019). The DeepMIP contribution to PMIP4: Methodologies for selection, compilation and analysis of latest Paleocene and early Eocene climate proxy data, incorporating version 0.1 of the DeepMIP database. *Geoscientific Model Development*, 12(7), 3149–3206. <https://doi.org/10.5194/gmd-12-3149-2019>
- Houben, A. J. P., Bijl, P. K., Sluijs, A., Schouten, S., & Brinkhuis, H. (2019). Late Eocene Southern Ocean cooling and invigoration of circulation preconditioned Antarctica for full-scale glaciation. *Geochemistry, Geophysics, Geosystems*, 20, 2214–2234. <https://doi.org/10.1029/2019GC008182>
- Huber, M., Brinkhuis, H., Stickley, C. E., Doos, K., Sluijs, A., Warnaar, J., et al. (2004). Eocene circulation of the Southern Ocean: Was Antarctica kept warm by subtropical waters? *Paleoceanography*, 19, PA4026. <https://doi.org/10.1029/2004PA001014>
- Huber, M., & Caballero, R. (2011). The early Eocene equable climate problem revisited. *Climate of the Past*, 7, 603–633. <https://doi.org/10.5194/cp-7-603-2011>

- Huber, M., & Nof, D. (2006). The ocean circulation in the southern hemisphere and its climatic impacts in the Eocene. *Palaeogeography, Palaeoclimatology, Palaeoecology*, 231, 9–28. <https://doi.org/10.1016/j.palaeo.2005.07.037>
- Huber, M., Sloan, L., & Shellito, C. (2003). *Early Paleogene oceans and climate: A fully coupled modeling approach using the NCAR CCSM*. Geological Society of America.
- Hutchinson, D. K., Coxall, H. K., Lunt, D. J., Steinthorsdottir, M., De Boer, A. M., Baatsen, M., et al. (2021). The Eocene-Oligocene transition: A review of marine and terrestrial proxy data, models and model-data comparisons. *Climate of the Past*, 17(1), 269–315. <https://doi.org/10.5194/cp-17-269-2021>
- Inglis, G., Farnsworth, A., Lunt, D., Foster, G., Hollis, C. J., Pagani, M., et al. (2015). Descent toward the Icehouse: Eocene Sea surface cooling inferred from GDGT distributions. *Paleoceanography and Paleoclimatology*, 30(7), 1000–1020. <https://doi.org/10.1002/2014PA002723>
- Kennedy-Asser, A. T., Lunt, D. J., Valdes, P. J., Ladant, J.-B., Frieling, J., & Laurentano, V. (2020). Changes in the high-latitude southern hemisphere through the Eocene-Oligocene transition: A model-data comparison. *Climate of the Past*, 16, 555–573. <https://doi.org/10.5194/cp-16-555-2020>
- Kirtman, B., Bitz, C., Bryan, F., Collins, W., Dennis, J., Hearn, N., et al. (2012). Impact of ocean model resolution on CCSM climate simulations. *Climate Dynamics*, 39, 1303–1328. <https://doi.org/10.1007/s00382-012-1500-3>
- Lanzante, J. R., Dixon, K. W., Nath, M. J., Whitlock, C. E., & Adams-Smith, D. (2018). Some pitfalls in statistical downscaling of future climate. *American Meteorological Society*, 99(4), 791–803. <https://doi.org/10.1175/BAMS-D-17-0046.1>
- Le Bars, D., Viebahn, J. P., & Dijkstra, H. A. (2016). A Southern Ocean mode of multidecadal variability. *Geophysical Research Letters*, 43, 2102–2110. <https://doi.org/10.1002/2016GL068177>
- Liu, Z., He, F., Brady, E. C., Tomas, R., Clark, P. U., Carlson, A. E., et al. (2009). Transient simulation of last deglaciation with a new mechanism for Bølling-Allerød warming. *Science*, 325, 310–314. <https://doi.org/10.1126/science.1171041>
- Lunt, D. J., Bragg, F., Chan, W. L., Hutchinson, D. K., Ladant, J. B., Morozova, P., et al. (2021). DeepMIP: Model intercomparison of early Eocene climatic optimum (EECO) large-scale climate features and comparison with proxy data. *Climate of the Past*, 17(1), 203–227. <https://doi.org/10.5194/cp-17-203-2021>
- Lunt, D. J., Jones, T. D., Heinemann, M., Huber, M., Legrande, A., Winguth, A., et al. (2012). A model-data comparison for a multi-model ensemble of early Eocene atmosphere-ocean simulations: EoMIP. *Climate of the Past*, 8, 1717–1736. <https://doi.org/10.5194/cp-8-1717-2012>
- Maltrud, M., Bryan, F., & Peacock, S. (2010). Boundary impulse response functions in a century-long eddying global ocean simulation. *Environmental Fluid Mechanics*, 10(1), 275–295. <https://doi.org/10.1007/s10652-009-9154-3>
- Marshall, D. (1994). Topographic steering of the Antarctic circumpolar current. *Journal of Physical Oceanography*, 25, 1636–1650.
- Marzocchi, A., Hirschi, J. J. M., Holliday, N. P., Cunningham, S. A., Blaker, A. T., & Coward, A. C. (2015). The North Atlantic subpolar circulation in an eddy-resolving global ocean model. *Journal of Marine Systems*, 142, 126–143. <https://doi.org/10.1016/j.jmarsys.2014.10.007>
- McClean, J., Bader, D., Bryan, F., Maltrud, M., Dennis, J., Mirin, A., et al. (2011). A prototype two-decade fully-coupled fine-resolution CCSM simulation. *Ocean Modelling*, 39, 10–30. <https://doi.org/10.1016/j.ocemod.2011.02.011>
- McClean, J. L., Maltrud, M. E., & Bryan, F. O. (2006). Measures of the fidelity of eddying ocean models. *Oceanography*, 19(1), 104–117. <https://doi.org/10.5670/oceanog.2006.94>
- Müller, V., Kieke, D., Myers, P. G., Pennelly, C., Steinfeldt, R., & Stendardo, I. (2019). Heat and freshwater transport by mesoscale eddies in the southern subpolar north Atlantic. *Journal of Geophysical Research: Ocean*, 124, 5565–5585. <https://doi.org/10.1029/2018JC014697>
- Munday, D. R., Johnson, H. L., & Marshall, D. P. (2015). The role of ocean gateways in the dynamics and sensitivity to wind stress of the early Antarctic circumpolar current. *Paleoceanography*, 30, 284–302. <https://doi.org/10.1002/2014PA002675>
- Nootboom, P. D. (2022a). pdnootboom/MCEocene: Code for 'improved model-data agreement with strongly eddying ocean simulations in the middle-late Eocene' by p. d. nootboom et al.(version v1) (v1.0.0). [Software]. Zenodo. <https://doi.org/10.5281/zenodo.6540852>
- Nootboom, P. D. (2022b). Pop data for nootboom et al., 2022. [dataset]. Yoda. Retrieved from <https://public.yoda.uu.nl/science/UU01/9N-FEKH.html>
- Nootboom, P. D., Bijl, P. K., van Sebille, E., von der Heydt, A. S., & Dijkstra, H. A. (2019). Transport bias by ocean currents in sedimentary microplankton assemblages: Implications for paleoceanographic reconstructions. *Paleoceanography and Paleoclimatology*, 34, 1178–1194. <https://doi.org/10.1029/2019PA003606>
- Nootboom, P. D., Delandmeter, P., Sebille, E. V., Bijl, P. K., Dijkstra, H. A., & von der Heydt, A. S. (2020). Resolution dependency of sinking Lagrangian particles in ocean general circulation models. *PLoS One*, 15(9), e0238650. <https://doi.org/10.1371/journal.pone.0238650>
- Porta Mana, P. G. L., & Zanna, L. (2014). Toward a stochastic parameterization of ocean mesoscale eddies. *Ocean Modelling*, 79, 1–20. <https://doi.org/10.1016/j.ocemod.2014.04.002>
- Pross, J., Contreras, L., Bijl, P. K., Greenwood, D. R., Bohaty, S. M., Schouten, S., et al. (2012). Persistent near-tropical warmth on the Antarctic continent during the early Eocene epoch. *Nature*, 488(7409), 73–77. <https://doi.org/10.1038/nature11300>
- Qin, X., van Sebille, E., & Sen Gupta, A. (2014). Quantification of errors induced by temporal resolution on Lagrangian particles in an eddy-resolving model. *Ocean Modelling*, 76, 20–30. <https://doi.org/10.1016/j.ocemod.2014.02.002>
- Rahmstorf, S., & Willebrand, J. (1995). The role of temperature feedback in stabilizing the thermohaline circulation. *Journal of Physical Oceanography*, 25, 787–805. [https://doi.org/10.1175/1520-0485\(1995\)025<0787:trotfi>2.0.co;2](https://doi.org/10.1175/1520-0485(1995)025<0787:trotfi>2.0.co;2)
- Rintoul, S. R. (2018). The global influence of localized dynamics in the Southern Ocean. *Nature*, 558, 209–218. <https://doi.org/10.1038/s41586-018-0182-3>
- Sauermilch, I., Whittaker, J., Klocker, A., Munday, D., Hochmuth, K., Bijl, P., & LaCasce, J. (2021). Gateway-driven weakening of ocean gyres leads to Southern Ocean cooling. *Nature Communications*, 12, 6465. <https://doi.org/10.1038/s41467-021-26658-1>
- Schmidt, G. A., Annan, J. D., Bartlein, P. J., Cook, B. I., Guilyardi, E., Hargreaves, J. C., et al. (2014). Using palaeo-climate comparisons to constrain future projections in CMIP5. *Climate of the Past*, 10, 221–250. <https://doi.org/10.5194/cp-10-221-2014>
- Scoccimarro, E., Gualdi, S., Bellucci, A., Sanna, A., Fogli, P. G., Manzini, E., et al. (2011). Effects of tropical cyclones on ocean heat transport in a high-resolution coupled general circulation model. *Journal of Climate*, 24(16), 4368–4384. <https://doi.org/10.1175/2011JCLI4104.1>
- Sijp, W. P., von der Heydt, A. S., & Bijl, P. K. (2016). Model simulations of early westward flow across the Tasman Gateway during the early Eocene. *Climate of the Past*, 12, 807–817. <https://doi.org/10.5194/cp-12-807-2016>
- Sijp, W. P., von der Heydt, A. S., Dijkstra, H. A., Flögel, S., Douglas, P. M. J., & Bijl, P. K. (2014). The role of ocean gateways on cooling climate on long time scales. *Global and Planetary Change*, 119, 1–22. <https://doi.org/10.1016/j.gloplacha.2014.04.004>
- Small, R., Bacmeister, J., Bailey, D., Bishop, S., Bryan, F., Caron, J., et al. (2014). A new synoptic scale resolving global climate simulation using the Community Earth System Model. *Journal of Advances in Modeling Earth Systems*, 6, 1065–1094. <https://doi.org/10.1002/2014MS000363>
- Smith, R., Jones, P., Briegleb, F., Bryan, F., Danabasoglu, G., Dennis, J., et al. (2010). *The Parallel Ocean Program (POP) reference manual ocean component of the Community Climate System Model (CCSM) and Community Earth System Model (CESM)* (p. 141). LAUR-01853.

- Stickley, C. E., Brinkhuis, H., Schellenberg, S. A., Sluijs, A., Fuller, M., Grauert, M., et al. (2004). Timing and nature of the deepening of the Tasmanian gateway. *Paleoceanography*, *19*, PA4027. <https://doi.org/10.1029/2004PA001022>
- Sun, B., Liu, C., & Wang, F. (2019). Global meridional eddy heat transport inferred from Argo and altimetry observations. *Scientific Reports*, *9*, 1345. <https://doi.org/10.1038/s41598-018-38069-2>
- Tabor, C. R., Poulsen, C. J., Lunt, D. J., Rosenbloom, N. A., Otto-Bliesner, B. L., Markwick, P. J., et al. (2016). The cause of late Cretaceous cooling: A multimodel-proxy comparison. *Geology*, *44*(11), 963–966. <https://doi.org/10.1130/G38363.1>
- Tierney, J. E., Poulsen, C. J., Montañez, I. P., Bhattacharya, T., Feng, R., Ford, H. L., et al. (2020). Past climates inform our future. *Science*, *370*(680). <https://doi.org/10.1126/science.aay3701>
- Tumoulin, A., Donnadieu, Y., Ladant, J. B., Batenburg, S. J., Poblete, F., & Dupont-Nivete, G. (2020). Quantifying the effect of the Drake Passage opening on the Eocene Ocean. *Paleoceanography*, *35*, e2020PA003889. <https://doi.org/10.1029/2020PA003889>
- van Hinsbergen, D. J. J., Groot, L. V. D., van Schaik, S. J., Spakman, W., Bijl, P. K., Sluijs, A., et al. (2015). A paleolatitude calculator for paleoclimate studies. *PLoS One*, *10*(6), e0126946. <https://doi.org/10.1371/journal.pone.0126946>
- Viebahn, J. P., von der Heydt, A. S., Le Bars, D., & Dijkstra, H. A. (2016). Effects of Drake Passage on a strongly eddying global ocean. *Paleoceanography*, *31*, 564–581. <https://doi.org/10.1002/2015PA002888>
- Waterman, S., Hogg, N. G., & Jayne, S. R. (2011). Eddy-mean flow interaction in the Kuroshio extension region. *Journal of Physical Oceanography*, *41*(6), 1182–1208. <https://doi.org/10.1175/2010JPO4564.1>
- Weijer, W., Maltrud, M. E., Hecht, M. W., Dijkstra, H. A., & Kliphuis, M. A. (2012). Response of the Atlantic Ocean circulation to Greenland Ice Sheet melting in a strongly-eddying ocean model. *Geophysical Research Letters*, *39*, L09606. <https://doi.org/10.1029/2012GL051611>
- Zhang, Z.-S., Qing, Y., & Wang, H.-J. (2010). Has the drake passage played an essential role in the cenozoic cooling? *Atmospheric and Oceanic Science Letters*, *3*(5), 288–292. <https://doi.org/10.1080/16742834.2010.11446884>
- Zhu, J., Poulsen, C. J., & Otto-bliesner, B. L. (2020). High climate sensitivity in CMIP6 model not supported by paleoclimate. *Nature Climate Change*, *1*, 378–379. <https://doi.org/10.1038/s41558-020-0764-6>